NASA-CR-196078

Numerical Modeling Studies of Wake Vortex Transport and Evolution Within the Planetary Boundary Layer

FY94 July Semi-Annual Report

(NASA-CR-196078) NUMERICAL MODELING STUDIES OF WAKE VORTEX TRANSPORT AND EVOLUTION WITHIN THE PLANETARY BOUNDARY LAYER Semiannual Report, FY 1994 (North Carolina State Univ.) 17 p

N94-35522

Unclas

G3/03 0013768

Yuh-Lang Lin
S. Pal Arya
Michael L. Kaplan

Department of Marine, Earth and Atmospheric Sciences
North Carolina State University
Raleigh, NC 27695-8208

1 Introduction

The most significant hazard associated with spacing of commercial aircraft when landing is the wing tip trailing vortex from the leading aircraft. The vorticity associated with the circulation that generates lift on a wing is continually shed and tends to roll up into a tight vortex aligned with the flight path. There are two of these vortices for a given aircraft, one associated with each wing. The air velocity fluctuations associated with these vortices are strong enough to pose a threat to following airplanes. Thus, the FAA regulations for spacing of aircraft at landing are intended to account for the decay of these vortices. This decay, however, is not well understood. As described by Stough et al. [1], the current FAA regulations depend on whether the prevailing conditions are VMC (visual meteorological conditions) or IMC (instrument meteorological conditions). Under VMC, it is up to the pilot of the following aircraft to maintain a safe distance, whereas FAA minimum spacing requirements must be adhered to under IFC. Thus, the only way in which the meteorological conditions are taken into account is in regard to the pilot's visual capabilities, not the dynamics of the trailing vortices. It is believed that with more knowledge of how trailing vortices decay under varying atmospheric conditions, air traffic capacity and safety may be increased.

Past research has primarily focused on how the trailing vortices move under stable or neutral atmospheric conditions. Greene's [2] analytical model compared well with the few laboratory and observational measurements available, but dealt only with wake vortices in the free atmosphere, not in the atmospheric boundary layer. Zheng and Ash [3] have had success with their numerical model predicting the motion of the vortices near the ground. In their case, however, only the turbulence associated with the vortices, themselves was considered. To date, there has not been a successful study describing the interaction of realistic atmospheric convective turbulence and the trailing vortex system. The goal of our research is to fill this gap.

We will use the TASS(Terminal Area Simulation System) model developed by Proctor [4] to study this problem. TASS is a non-hydrostatic Large Eddy Simulation model which includes parameterizations for hydrometeors.

2 Objectives and goals of the research

The proposed research involves four tasks. The first of these is to simulate accurately the turbulent processes in the atmospheric boundary layer. TASS was originally developed to study meso-γ scale phenomena, such as tornadic storms, microbursts and windshear effects in terminal areas. Simulation of wake vortex evolution, however, will rely on appropriate representation of the physical processes in the surface layer and mixed layer. This involves two parts. First, a specified heat flux boundary condition must be implemented at the surface. Using this boundary condition, simulation results will be compared to experimental data and to other model results for validation. At this point, any necessary changes to the model will be implemented. Next, a surface energy budget parameterization will be added to the model. This will enable calculation of the surface fluxes by accounting for the radiative heat transfer to and from the ground and heat loss to the soil rather than simple specification of the fluxes.

The second task involves running TASS with prescribed wake vortices in the initial condition. The vortex models will be supplied by NASA Langley Research Center. Sensitivity tests will be performed on different meteorological environments in the atmospheric boundary layer, which include stable, neutral, and unstable stratifications, calm and severe wind conditions, and dry and wet conditions. Vortex strength may be varied as well. Relevant non-dimensional parameters will include the following: Richardson number or Froude number, Bowen ratio, and height to length scale ratios. The model output will be analyzed and visualized to better understand the transport, decay, and growth rates of the wake vortices.

The third task involves running simulations using observed data. MIT Lincoln Labs is currently planning field experiments at the Memphis airport to measure both meteorological conditions and wake vortex characteristics. Once this data becomes available, it can be used to validate the model for vortex behavior under different atmospheric conditions. The fourth task will be to simulate the wake in a more realistic environment covering a wider area. This will involve grid nesting, since high resolution will be required in the wake region but a larger total domain will be used.

During the first allocation year, most of the first task will be accomplished.

3 Work accomplished during the period 1/94-6/94

3.1 Surface energy balance scheme

The parameterizations to be used in the surface energy balance have been determined. A description of these parameterizations follows.

The surface energy balance may be described as:

$$\Delta Q_s = Q^* - Q_g - Q_H - Q_E \tag{1}$$

where ΔQ_s represents the rate of change in energy storage in the surface layer of the soil per unit area, Q^* the net radiative flux to the ground, Q_g the heat loss to the deep soil, Q_H the sensible heat flux to the atmosphere, and Q_E the latent heat flux to the atmosphere.

The radiative flux may be broken down in the following way:

$$Q^* = K + L\downarrow - L\uparrow \tag{2}$$

where $L\downarrow$ is the longwave incoming radiation and $L\uparrow$ is the longwave outgoing radiation. K is the net shortwave radiation and may be written as

$$K = T_K S(1 - A)\sin\Psi \tag{3}$$

where S is the solar radiation at the top of the atmosphere, A is the albedo, and T_K is the atmospheric transmissivity. Ψ is the solar elevation angle and may be expressed as

$$\sin\Psi = \sin\phi\sin\delta_s - \cos\phi\cos\delta_s\cos[(\frac{\pi t_{UTC}}{12}) - \lambda_e]. \tag{4}$$

In this formulation, ϕ is the latitude, λ_e the longitude, δ_s the solar declination, and t_{UTC} the standard time of day at 0^o longitude.

Burridge & Gadd [5] parameterize the transmissivity as

$$T_K = (0.6 + 0.2\sin\Psi)(1 - 0.4\sigma_{C_H})(1 - 0.7\sigma_{C_M})(1 - 0.4\sigma_{C_L}) \tag{5}$$

where σ_{C_H}, σ_{C_M}, and σ_{C_L} represent high, middle, and low cloud fraction, respectively.

We may express the outgoing longwave radiation as

$$L\uparrow = \epsilon\sigma T_g^4 \tag{6}$$

where ϵ is the emissivity of the ground, σ the Stefan-Boltzmann constant, and T_g the ground temperature.

Staley & Jurica [6] parameterized the incoming longwave radiation as

$$L \downarrow = [\sigma_c + (1 - \sigma_c)(0.67)(1670 q_a)^{0.08}]\sigma T_a^4 \tag{7}$$

where σ_c is the total cloud cover, q_a is the humidity at the surface reference level of the *atmosphere* (usually about ten meters), and T_a is the air temperature at that level.

By Monin-Oboukov scaling, the sensible heat flux to the atmosphere is

$$Q_H = \rho c_p u_* \theta_* \tag{8}$$

where

$$u_* = \frac{k u_a}{\{\ln(\frac{z_a}{z_0}) - \psi_M(\frac{z_a}{L})\}} \tag{9}$$

and

$$\theta_* = \frac{k(\theta_a - \theta_g)}{\{\ln(\frac{z_a}{z_0}) - \psi_H(\frac{z_a}{L})\}}. \tag{10}$$

Here k represents Von Karmann's constant, z_0 the roughness length, L the Monin-Obukhov length (which depends upon stability), and ψ_M and ψ_H are stability dependent functions related to the dimensionless wind shear and potential temperature gradient. u_a and θ_a are the velocity and potential temperature, respectively, at the reference level in the surface layer, and θ_g is the potential temperature at the ground.

There are two remaining terms on the right hand side of Equation 1, Q_g and Q_E. To determine these, we will use a slab model of the soil which was developed by Bhumralkar [7]. Deardorff [8] showed that this was a very accurate method. In addition, it is much more efficient than numerically solving the heat conduction equation with many layers within the soil. As shown in Figure 1, the soil is modeled as two layers: a slab in which the temperature changes throughout the day, and a substrate in which the temperature remains constant throughout the diurnal period. The amount of heat energy in the ground slab lost to the substrate is

$$Q_g = \frac{2\pi \rho_s d_1 c_s}{\tau_1}(T_g - T_m). \tag{11}$$

Here, ρ_s is the soil density, c_s is the soil heat capacity, d_1 is the depth of the ground slab, T_g is the temperature of the ground slab, T_m is the temperature

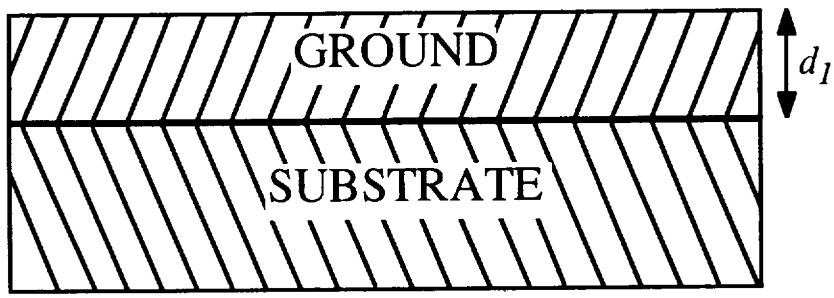

Figure 1: Schematic drawing of slab soil model.

of the substrate, and τ_1 is the diurnal period (twenty-four hours). The rate of change of the energy contained within the ground slab (the left hand side of Equation 1) is then

$$\Delta Q_s = \rho_s c_s d_1 \frac{\partial T_g}{\partial t} \tag{12}$$

In a manner similar to Equation 8, we may define the latent heat flux to the atmosphere as

$$Q_E = -\rho L_e u_* q_* \tag{13}$$

where L_e is the latent heat of evaporation,

$$q_* = \frac{k(q_a - q_g)}{\{\ln(\frac{z_a}{z_0}) - \psi_H(\frac{z_a}{L})\}}, \tag{14}$$

and q_a and q_g are the specific humidity at the surface and ground level, respectively. Using Deardorff's [8] parameterization,

$$q_a - q_g = \alpha'[q_a - q_{sat}(T_s)] \tag{15}$$

where $q_{sat}(T_s)$ is the saturation specific humidity at the ground temperature and

$$\alpha' = \min(1, \frac{w_s}{w_k}). \tag{16}$$

Here, w_s is the volume fraction of soil moisture in the ground slab and w_k is the soil moisture fraction above which the ground acts as if it were saturated. We may then write

$$\frac{\partial w_g}{\partial t} = C_1(E_g - P) - C_2\frac{(w_s - w_m)}{\tau_1} \quad (17)$$

where E_g is the evaporation, P the precipitation, and w_m the moisture fraction in the substrate. C_1 and C_2 are empirical constants.

After we are convinced that TASS gives the proper results with a given surface heat and moisture flux, this surface energy parameterization will be tested with data from Ripley & Redmann [9], which includes measurements of u_a, Q^*, Q_g, Q_E, and Q_H. We will prescribe the shortwave radiative flux, the surface wind, the stability, moisture, and the deep substrate temperature to match the experiment and follow the development of T_s, Q_E, and Q_H. We will then add this parameterization to the TASS model.

3.2 Large eddy simulations of the atmospheric boundary layer

Since May 18, 1994, Dr. David Schowalter and Mr. David DeCroix have been in residence at NASA Langley Research Center learning how to use the TASS model under the direction of Dr. Fred Proctor. They will remain there until mid-August. What follows has been accomplished there in the first month.

In order to validate model results for simulation of the atmospheric boundary layer, a surface heat flux boundary condition has been added to the model. The surface heat flux in this case is a function of the time of day. The model has been tested with input data from the Wangara field experiment [10]. We are using data from Day 33 to test mean quantities against experimental values. The surface heat flux for this case was not measured and was obtained from Deardorff's [11] model. Only instantaneous values of velocity and temperature are available from this observational data set for altitudes above $16m$. Thus, we are comparing turbulent quantity results with Deardorff [11] and other modelers who tested large eddy simulation output against the same experimental data.

Figure 2 shows a comparison of potential temperature profiles as a function of the time of day. The simulation was initialized with the profile shown at 9:00, which matched the experimental data exactly. A 40×40×40 grid was used for the internal domain. Periodic horizontal boundary conditions were

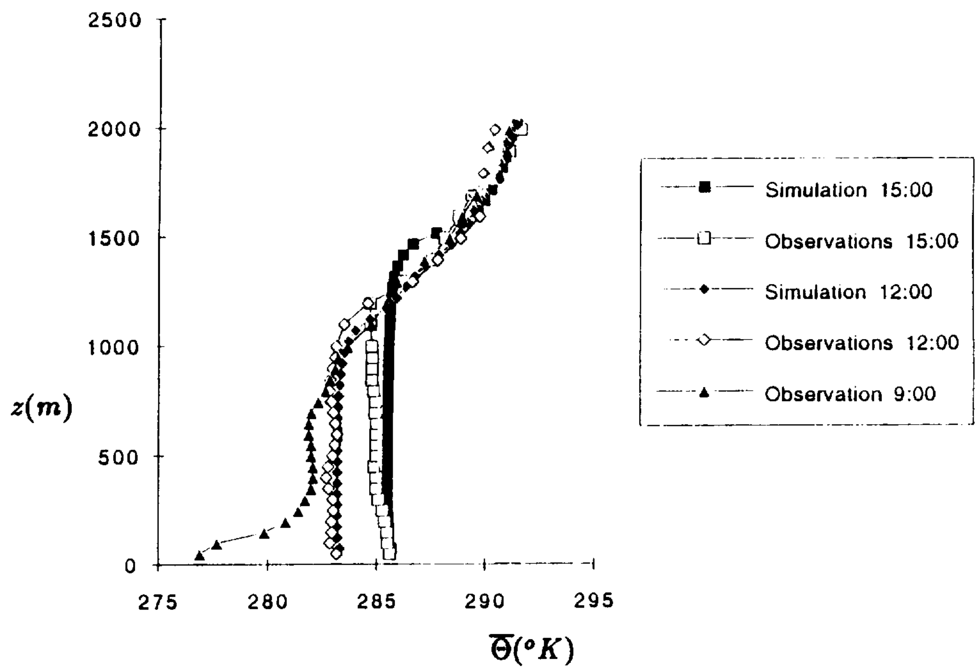

Figure 2: Variation of potential temperature throughout the day. Comparison is with data from the Wangara Experiment, Day 33.

used with a rigid lid and sponge condition at the top boundary. The domain covered a region $5Km \times 5Km \times 2Km$, the latter dimension representing the domain height. This corresponds to $125m$ resolution horizontally and $50m$ vertically. This resolution corresponds to that used by Deardorff, which was desirable for comparison purposes. The simulated profiles at 12:00 and 15:00 compare well with the data. It is important to note, however, that our results show slightly higher temperatures at the top of the mixed layer and a larger mixed layer height than those measured at 15:00. Deardorff's LES model results show similar discrepancies. This is most probably due to large scale advection and subsidence taking place during the observations. These synoptic effects are not accounted for in the current model, though it may be in the future if deemed necessary.

Figure 3 reveals contours of vertical velocity in a vertical plane at 14:00 (2:00 p.m.) for the Wangara simulation. Thermal plumes can be seen quite clearly. It should be mentioned at this point that the size of visible turbulent eddies is limited on the small scale end by the resolution of the grid (125 m in the horizontal). The thermals shown here have a typical horizontal size

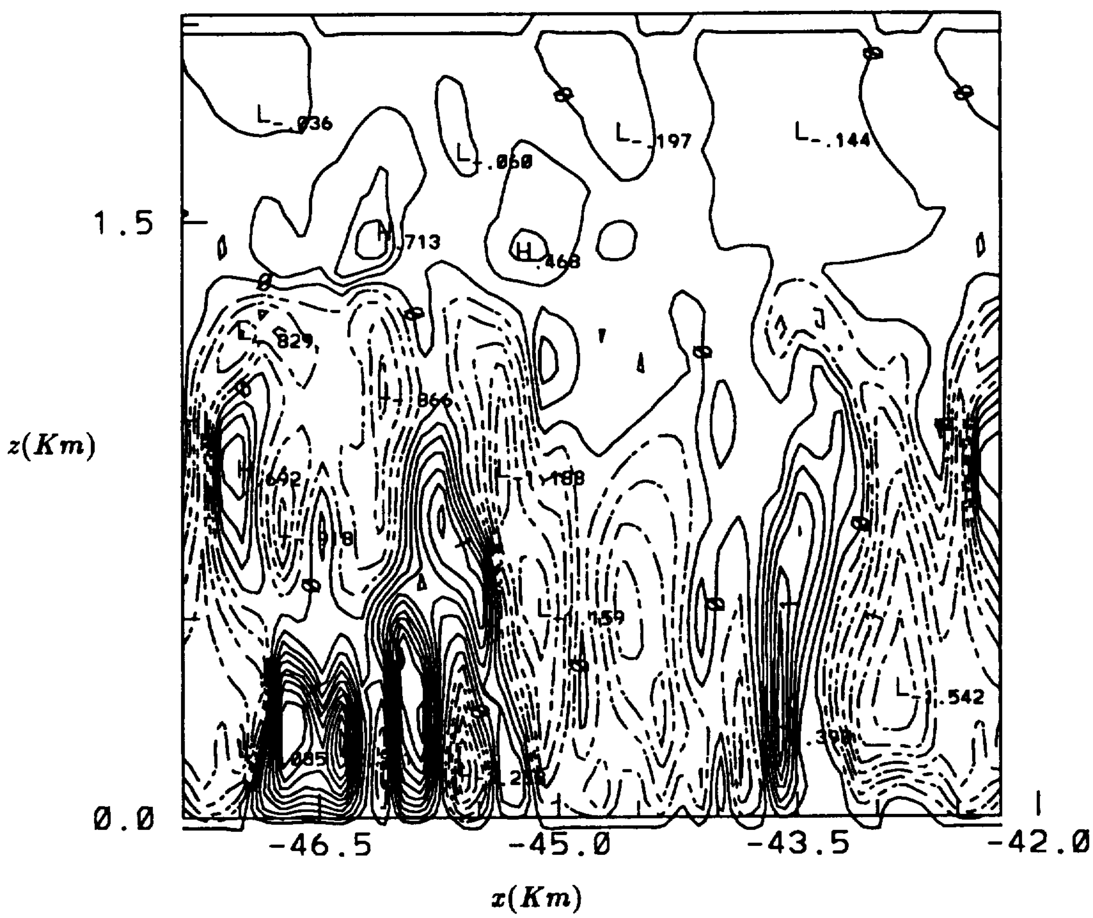

Figure 3: Vertical plane showing contours of vertical velocity w at $t = 14:00$ for the Wangara simulation. Contours are from -1.4 m/s to 2.2 m/s by 0.2. Negative contours are shown with dashed curves.

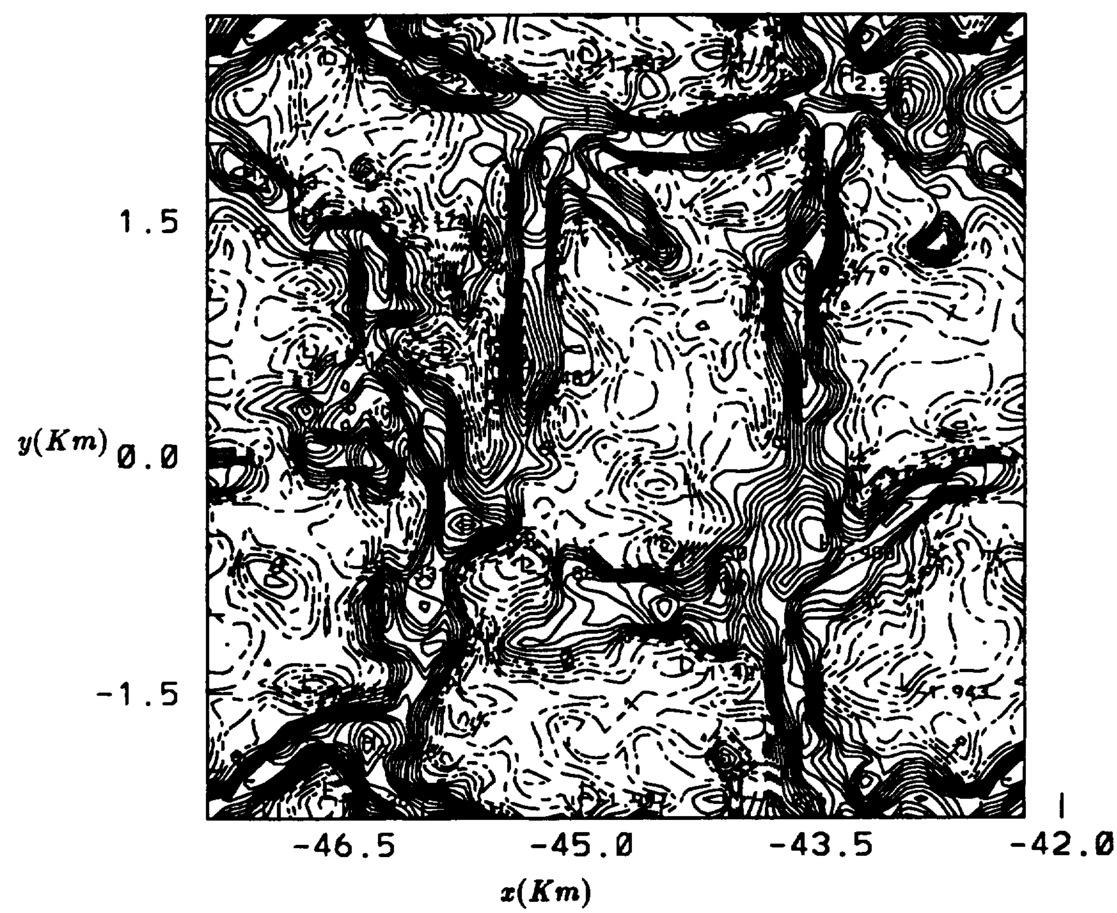

Figure 4: Horizontal plane showing contours of vertical velocity w at t = 14 : 00 and at a height of z = 199m. Contours are from -2.0 m/s to 3.25 m/s by 0.25. Negative contours are shown with dashed curves.

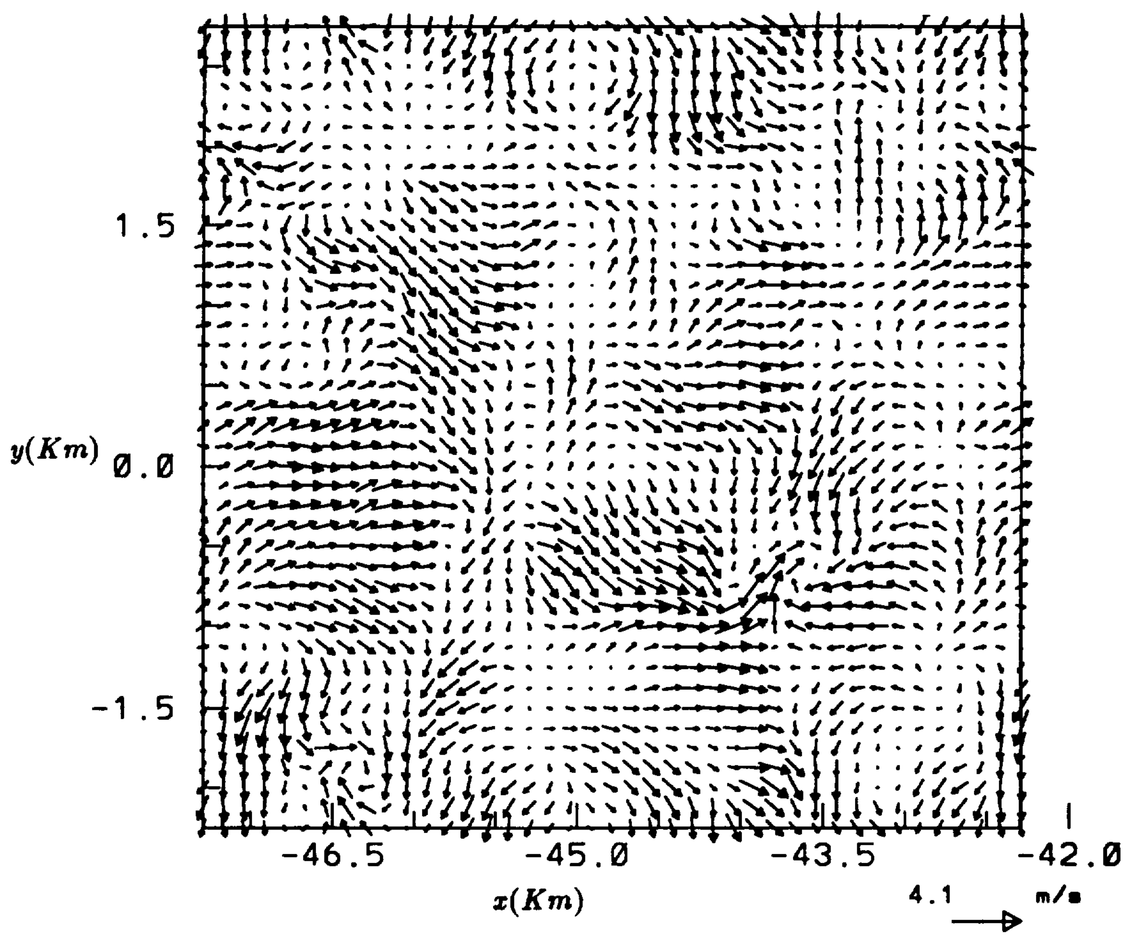

Figure 5: Same as Figure 4, but showing horizontal velocity vectors at $z = 224m$.

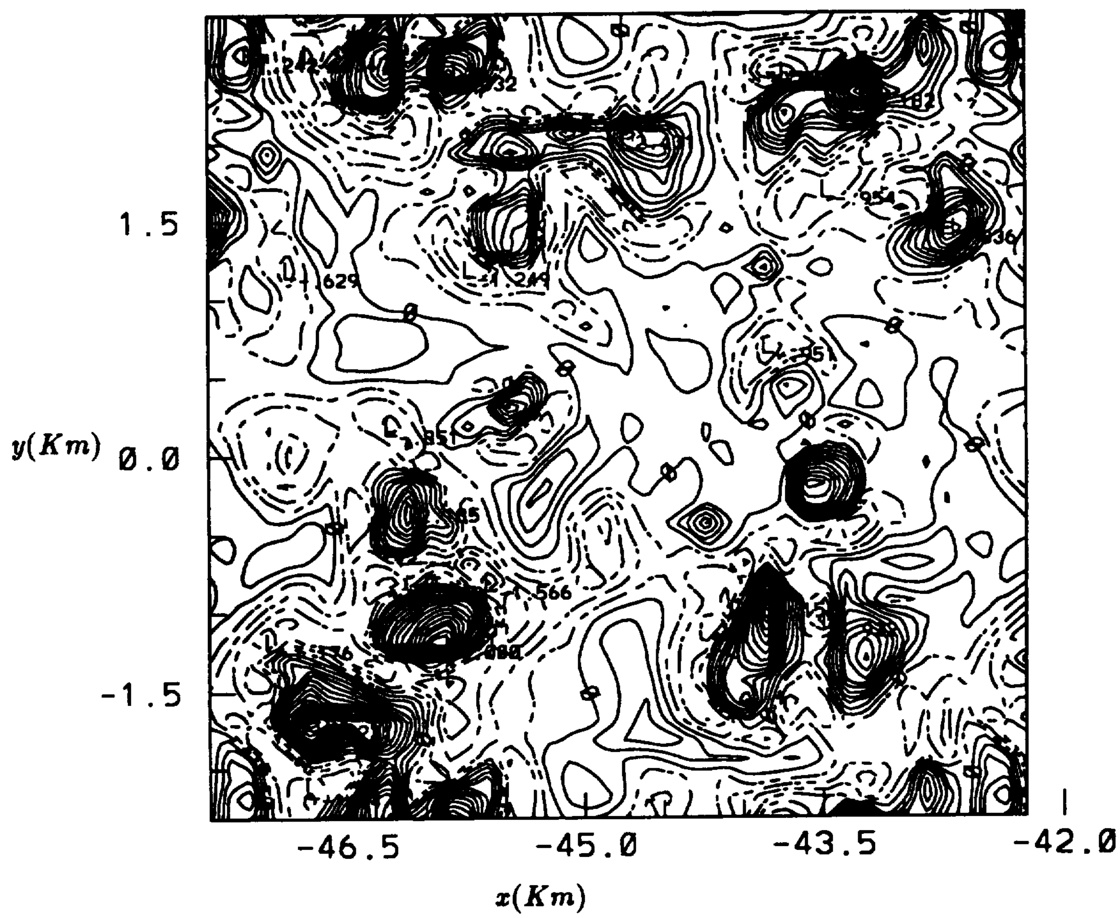

Figure 6: Horizontal plane showing contours of vertical velocity w at t = 14 : 00 and at a height of z = 1149m. Contours are from -1.5 m/s to 4.25 m/s by 0.25. Negative contours are shown with dashed curves.

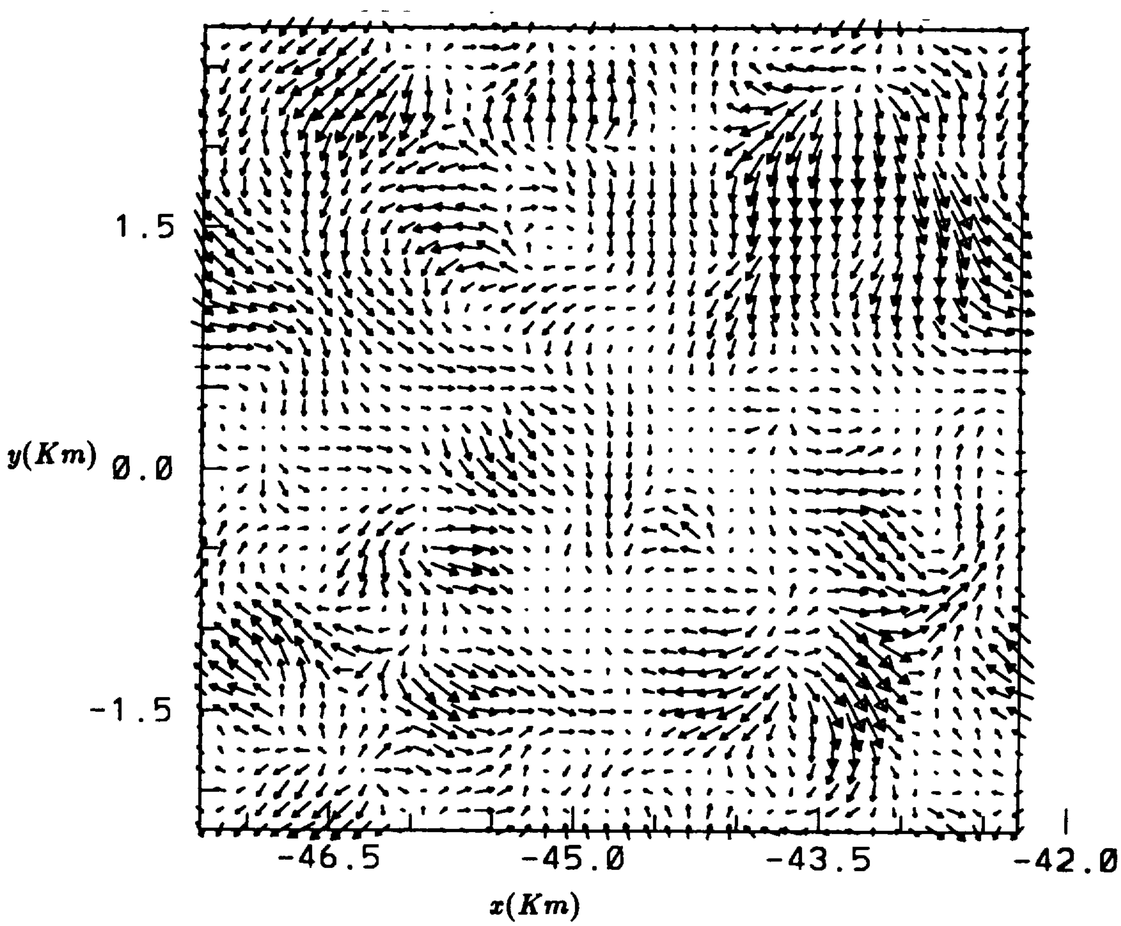

Figure 7: Same as Figure 6, but showing horizontal velocity vectors at $z = 1174m$.

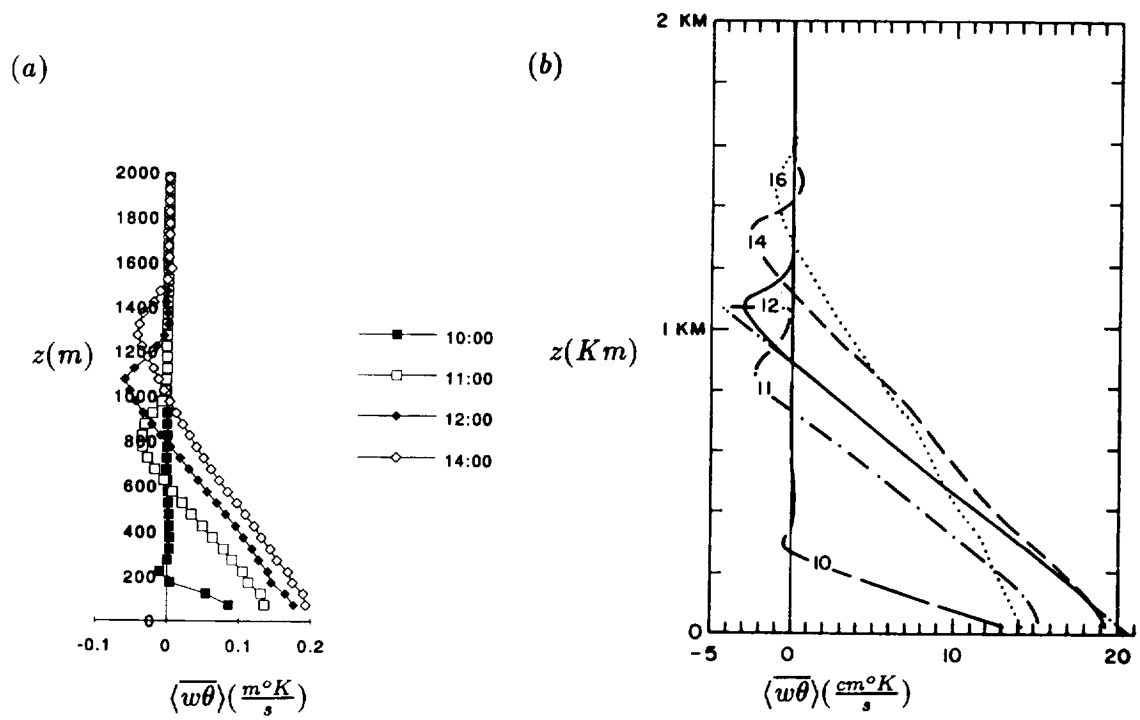

Figure 8: Sensible heat flux profiles as a function of local time of day. (*a*) Current results. (*b*) Results from Deardorff [11].

of roughly three grid cells. Thus, it is possible that the characteristic size of eddies would be smaller if a smaller grid size were used. These types of sensitivity tests will be done in the future. These thermals can be observed from above, as well, as in Figure 4, which shows a horizontal plane of vertical velocity contours. Figure 5 shows the horizontal velocity vectors at nearly the same height. Careful observation will show that at this altitude, the thermals are associated with horizontal convergence. Figures 6 and 7 show similar contours and vectors, but higher up in the boundary layer ($1149m$ and $1174m$, respectively) where the thermals are less intense. At this higher altitude, there is divergence associated with the thermal plumes. Fundamentally, then, the simulation gives a realistic representation of boundary layer processes.

In figure 8, we compare the sensible heat flux profiles (not measured in the experiment) with Deardorff's results. Qualitatively, they are very similar, though the heat flux minimum in these curves has a slightly lower value in our case. Because we are comparing model to model, however, it is very difficult to determine which results are correct. It is important, therefore, to compare turbulent quantities with observational data.

4 Work in progress and objectives for the period 7/94-10/94

Because we believe that the wake vortex development will be sensitive to atmospheric turbulence, it is important to test turbulent quantities in addition to mean values. The Wangara data does not include these measurements, so it is necessary to turn to the Minnesota field experiment [12]. Most importantly, we will compare variances of velocity and temperature as well as turbulent fluxes of heat, moisture, and momentum between the model and the experiment. Not only is this a useful test of the TASS model specifically, but of large eddy simulation in general. To our knowledge, no one has done an exhaustive comparison between atmospheric turbulence data and large eddy simulation results in the past.

After these tests are performed, we will add the surface energy balance to the model so that the surface fluxes will be determined by the amount of solar radiation reaching the ground and by the heat transfer through the soil. This work will be under way by the end of the allocation period (October 31, 1994). The first task is expected to be completed entirely in March, 1995.

References

[1] Stough, H. P. III, Greene, G. C., Stewart, E. C., Stuever, R. A., Jordan, F. L. Jr., Rivers, R. A., & Vicroy, D. D., 1993. NASA wake vortex research. AIAA 93-4004, Aircraft Design, Systems and Operations Meeting, Monterey, CA.

[2] Greene, G. C. 1986. An approximate model of vortex decay in the atmosphere. *J. Aircraft* **23**, pp. 566-573.

[3] Zheng, Z. & Ash, R .L. 1993. Prediction of turbulent wake vortex motion near the ground. *FED* **151**, pp. 195-207.

[4] Proctor, F. H. 1987. The Terminal Area Simulation System Volume I: Theoretical Formulation. NASA Contractor Report 4046 DOT/FAA/PM-86/50,I.

[5] Burridge, D. M., & Gadd, A. J. 1974. The Meteorological Office Operational 10 Level Numerical Weather Prediction Model (December 1974). British Met. Office Tech. Notes Nos. 12 and 48. London R., Bracknell, Berkshire, RG12 2SZ, England.

[6] Staley, D. O., & Jurica, G. M. 1972. Effective atmospheric emissivity under clear skies. *J. Appl. Meteorol.*, **11**, pp. 349-356.

[7] Bhumralkar, C. M. 1975. Numerical experiments on the computation of ground surface temperature in an atmospheric general circulation model, *J. Appl. Meteorol.*, **14**, pp. 1246-1258.

[8] Deardorff, J. W. 1978. Efficient prediction of ground surface temperature and moisture, with inclusion of a layer of vegetation. *JGR* **83**(C4), p. 1889.

[9] Ripley, E.A. & Redmann, R.E. 1976. Grassland. In "Vegetation and the Atmosphere Volume 2: Case Studies," J. L. Monteith, ed. Academic Press.

[10] Clarke, R. H., Dyer, A. J., Brook, R. R., Reid, D. G., & Troup, A. J., 1971. The Wangara Experiment: Boundary Layer Data. CSIRO Div. of Meteorol. Phys. Tech. Paper No. 19.

[11] Deardorff, J. W. 1974. Three-dimensional numerical study of the height and mean structure of a heated planetary boundary layer. *Boundary Layer Met.* 7 pp. 81-106.

[12] Izumi, Y. & Caughey, S. J. 1976. Minnesota 1973 Boundary Layer Data Report. Environmental Research Paper No. 547, AFGL, Bedford, MA.